Atomistic simulation of Mg_2SiO_4 and Mg_2GeO_4 spinels: a new model

M. Blanchard[1], K. Wright[1,2,3], J.D. Gale[3]

[1] Royal Institution of Great Britain, 21 Albemarle street, London W1S 4BS, UK

[2] Departments of Chemistry and Earth Sciences, University College London, Gower street, London WC1E 6BT, UK

[3] Nanochemistry Research Institute, Department of Applied Chemistry, Curtin University of Technology, P.O. Box U1987, Perth 6845, Western Australia

Communicating Author: Marc Blanchard

e-mail: marc@ri.ac.uk

Tel.: +44 (0)20 7409 2992

Fax: +44 (0)20 7629 3569

Abstract. We have developed a new interatomic potential model for the simulation of ringwoodite, the high-pressure phase of Mg_2SiO_4, and its low-pressure analogue, Mg_2GeO_4 spinel. The main novelty is the addition of a breathing shell model that enables us to accurately describe the structural and elastic parameters of both spinels up to 15 GPa. Our model has also been applied to the two other Mg_2SiO_4 polymorphs in order to test its transferability. We find that although it is able to reproduce the structure and physical properties of wadsleyite, the breathing shell description is less successful with forsterite. The Mott-Littleton method has been used to calculate the energy of the intrinsic point defects in both spinels. The results indicate that these phases are likely to have the same defect population with the MgO partial Schottky defect predominating.

Keywords Ringwoodite, Magnesium spinel, Atomistic simulation, Breathing shell model.

Introduction

The three $(Mg,Fe)_2SiO_4$-polymorphs, olivine, wadsleyite and ringwoodite, are major constituents of the Earth's mantle. Ringwoodite (γ-Mg_2SiO_4) is considered to be the most abundant mineral in the lower part of the transition zone (520-660 km depth) and therefore should be responsible for the physical and chemical properties of the mantle in this region. The germanate spinel (γ-Mg_2GeO_4) is stable at atmospheric pressure below 810°C as well as high pressure (Dachille and Roy 1960) and has been used as a low-pressure analogue for studying the olivine-spinel transition (Ringwood 1975).

Computer modelling techniques have a key role to play in predicting the physical and chemical properties of complex silicates that are not readily available from laboratory experiments. Information from calculations can also be used to aid in the interpretation of experimental data. For more than two decades, classical atomistic simulations, using interatomic potentials have been successfully used to model both the perfect and defective lattice properties of a wide range of materials (e.g. Lewis et al. 1985; Leslie 1989; Catlow and Price 1990; Purton and Catlow 1990; Wright et al. 1995; Walker et al. 2003). There have been numerous simulation studies of the stability and defect properties of olivine (e.g. Wright and Catlow 1994, Brodholt 1997) and wadsleyite (Wright and Catlow 1996, Haiber et al. 1997) although ringwoodite has received much less attention. Early simulations by Price et al. (1987) successfully used interatomic potentials derived for olivine to model the phase stability of the Mg_2SiO_4 polymorphs. However, these potentials were not able to reproduce the experimentally determined elastic properties of ringwoodite, which are essential if we wish to accurately model defect behaviour in this phase. The aim of the current study is to use atomistic methods to determine the properties of hydrogen defects in both ringwoodite and germanate spinel and thereby assess the usefulness of the germanate as an analogue material. However, in order to

achieve this aim it is first necessary to develop a set of interatomic potentials that will accurately describe the structure and properties of the two spinel-phases. Here, we describe the derivation of these potentials. Indeed, for this kind of simulation, results are particularly sensitive to the interatomic potentials used. Hence, the bulk structure and the perfect lattice properties must be described as perfectly as possible before adding defects. Once this step is successfully achieved, we will investigate the population of intrinsic defects in both spinels. The knowledge of the defect population is important because point defects control most of the physical properties of crystals (e.g. diffusion, electrical conductivity, creep) and for our subject of interest, the incorporation of hydrogen could not occur in these nominally anhydrous minerals without the presence of point defects.

In the following sections, we will first give details of the theoretical basis for our model and show how it was derived. We briefly describe the previous available models, present the changes adopted, and the accuracy gained, for the description of the spinel phase. Then, we will discuss the transferability of this new model to the other Mg_2SiO_4 polymorphs and the elastic behaviour under pressure. Finally, we will use the Mott-Littleton method to calculate the formation energies of the intrinsic point defects.

Methodology

Computer simulation methods are based on the determination of the energy of a solid as a function of the interaction of all the constituting particles. In classical atomistic simulations, the lattice energy of the system can be expressed as the sum of the interactions between the atoms, or ions, and these interactions are described by potential functions. We work within the framework of the Born model of solids, with the extension to polarizable ions.

Previous studies

Prior work that has considered the application of classical atomistic modelling to ringwoodite, has been concerned with the perfect lattice structure and properties of the Mg_2SiO_4 polymorphs. To our knowledge, the studies of Price and Parker, and, Matsui and Busing were the first, both in 1984. Three years later, Price et al. (1987) improved their forcefield model and applied it to the Mg_2SiO_4 polymorphs. Since then, this model has been used in both defect and diffusion studies of forsterite and wadsleyite (Wright and Catlow 1994, 1996; Walker et al. 2003). To date, these represent the only available sets of interatomic potentials for ringwoodite for static lattice simulations.

Here we briefly define the functional form of the interatomic potentials employed in previous works; this also forms the starting point for the derivation of the present model. The dominant contribution to the lattice energy for ionic materials, such as those being considered here, is the electrostatic energy. Treating all species as point particles, the Coulomb contribution is evaluated using an Ewald summation in order to achieve convergence to the zero dipole limit. In addition, it is necessary to include short-range interactions to model the repulsion between the electron clouds, as well as the Van der Waal's attraction due to dispersion. The two-body component of these interactions can be expressed in the form of the Buckingham potential:

$$U_{ij} = A\, exp\left(-\frac{r_{ij}}{\rho}\right) - \frac{C}{r_{ij}^6}, \qquad (1)$$

where $\underline{r}_{ij}$ is the distance between two atoms i and j. The parameters $\underline{A}$, $\underline{\rho}$ and $\underline{C}$, as well as the other potential parameters, can be derived either by recourse to *ab initio* quantum mechanics or by empirical fitting to the structural data and physical properties of simple binary oxides. The latter solution was adopted by Price et al. (1987). A three-body potential is added in order to describe the directionality of the O-Si-O bonds:

$$U_{ijk} = \frac{1}{2} k_{ijk} \left(\theta_{jik} - \theta_0\right)^2, \quad (2)$$

where $\underline{k_{ijk}}$ is a spring constant, $\underline{\theta_{jik}}$, the angle between the two interatomic vectors j-i and i-k (i.e. the O-Si-O bond angle), and $\underline{\theta_0}$ the tetrahedral angle. Finally, the ionic polarisability of the oxygen atoms is described by the simple, mechanical, shell model of Dick and Overhauser (1958). In this description, the core and the massless shell, representing the outer valence electron cloud, are allowed to have a distinct position separated by the distance, $\underline{r_i}$, and are coupled by a harmonic spring, $\underline{k}$:

$$U_i = \frac{1}{2} k_i r_i^2 \quad (3)$$

Values of the potential parameters used are given in Table 1 of the paper of Price et al. (1987). The results provided by this model for ringwoodite are reported in Table 1. The cell parameter is in good agreement with the experimental value, but the errors for the elastic constants are significant. For centrosymmetric cubic systems, like ringwoodite, the theoretical elastic constants must obey the Cauchy relation, $\underline{C_{44}} = \underline{C_{12}}$, when considering only central forces at zero stress, as is the case for all the existing potential models. However, experimentally the elastic behaviour of ringwoodite is characterized by a Cauchy violation ($\underline{C_{44}} \neq \underline{C_{12}}$) and this many-body effect cannot be reproduced with such a model. Aside from the Cauchy violation, even by fitting the previous potential parameters specifically to the experimental data for ringwoodite, it is not possible to achieve a satisfactory compromise between describing the unit cell volume and the elastic behaviour. Consequently, the use of an alternative model is explored in the present work..

New potential model

In this section, we describe the new potential model developed to better reproduce the elastic behaviour of ringwoodite, while maintaining an accurate description of the structure. The two-body interactions are still represented by the combination of the Coulomb energy and a

Buckingham potential, since this formulation has proven to be effective for many different ionic materials. The main change relates to the description of the oxygen polarisation. As is well documented (Gale 1997), for low-symmetry structures, the dipolar shell model is sufficient to absorb most of the effects of partial covalency/ionic polarisation, whereas for high-symmetry systems, a breathing shell model (Schroeder 1966) may be needed to represent the contribution of higher-order charge deformations of the oxide species. In the breathing shell model, the ion shell has a finite radius, R_0, which is allowed to deform isotropically under the influence of the other ions (Fig. 1). Here the ion size is coupled to the environment through the short-range repulsive potential acting upon the radius of the shell, rather than its centre. Equation (3) is still valid to treat the core-shell dipolar contribution, but an additional potential, which has been chosen to be harmonic, describes the breathing shell:

$$U_i = \frac{1}{2} K_i \left(R_i - R_0\right)^2 \tag{4}$$

where $\underline{K_i}$ is a spring constant and $\underline{(R_i\text{-}R_0)}$ is the distance from the finite shell radius of the ion i. The most significant consequence of the introduction of a breathing shell model is that, by introducing non-central forces, it is able to reproduce the Cauchy violation ($\underline{C_{44}} \neq \underline{C_{12}}$). Finally, we have also changed the three-body potential treating the O-Si-O bending (Eq. 2), because of the occurrence of abnormal coordination number for the silicon. We have chosen to employ the three-body potential of Stillinger and Weber since it tends to zero at the cut-off distance (Stillinger and Weber 1985):

$$U_{ijk} = k_{ijk}\ exp\left(\frac{\rho_{ij}}{r_{ij} - r_{ij}^{cutoff}} - \frac{\rho_{ik}}{r_{ik} - r_{ik}^{cutoff}}\right)\left(cos\left(\theta_{jik}\right) - cos\left(\theta_0\right)\right)^2 \tag{5}$$

where $\underline{k_{ijk}}$, $\underline{\rho}$, $\underline{r}$ and $\underline{\theta_{jik}}$ have the same meaning as before. This potential is known to give a reasonable description of crystalline silicon. Indeed, with the addition of bond length dependence in the exponential term, it discourages the formation of anything other than four-coordinate silicon.

The approach we have taken to describe the oxygen polarizibility is not the only one, and alternative strategies are available (e.g. Madden and Wilson 1996) that have been successful in transferring between different systems. However, they have not been used in the current study.

Results and discussion

The ability of the breathing shell model to reproduce the Cauchy violation has already been demonstrated for the case of magnesium oxide (e.g. Catlow et al. 1976). Therefore the breathing shell model of MgO was the starting point for the derivation of the potential parameters. All the parameters were then fitted to the experimentally determined structure and elastic properties of ringwoodite (Sasaki et al. 1982; Weidner et al. 1984) and the germanate spinel (Von Dreele et al. 1977; Weidner and Hamaya 1983), using the relaxed fitting approach within the GULP3.0 code (Gale 1997; Gale and Rohl 2003). Thus, the potential parameters were fitted to five constraints for each spinel. Only two parameters are required to describe the spinel structure: the lattice parameter, *a*, and the fractional coordinate of the oxygen at the special position (*u, u, u*). While the three other parameters correspond to the elastic constants, C_{11}, C_{12}, C_{44}. The full set of derived parameters is displayed in Table 2. Tables 1 and 3 give the results for ringwoodite and magnesium germanate, respectively. With differences always below 1 %, the agreement between calculated and experimental data is very good for both spinels. At zero pressure and zero temperature, the potentials employed enable us to describe very accurately the elastic constants and moduli, as well as the crystal structure. We also show in Table 4 the results of the calculations for periclase (MgO). They are in good agreement with the measurements of the cell parameter and elastic constants. This corresponds to an "a posteriori" test since this phase is known to present a strong Cauchy violation with a measured $\underline{C_{44}}/\underline{C_{12}}$ ratio reaching 1.64 (Yoneda

1990). Futhermore, the modelling of periclase will be necessary, in the following, in order to get its lattice energy, which in turn will be used to determine the energy of the partial MgO Schottky defect.

Mg_2SiO_4-polymorphs

We have demonstrated that the new model accurately describes the structure and the elastic behaviour of ringwoodite. We now turn to the two other Mg_2SiO_4 polymorphs, and compare our calculated properties with those from experiment and with those of the theoretical study of Price et al. (1987). The results are presented in Table 5. At first glance, the structure of forsterite seems to be well described by both models, with cell parameters being reproduced to within 2% of the measured value. However, the lengthening of a and shortening of c predicted by our model cause the structure to distort, giving negative phonon frequencies at the gamma point. These imaginary phonon modes indicate that the structure is unstable and wants to lower its symmetry, mainly in the b direction. If we now look at wadsleyite, the new model displays good results for the description for the unit cell, with the largest difference equal to 1.3 % along the c axis, while the elastic behaviour shows discrepancies of around 11 - 12 % for the bulk and shear moduli. These results are as good as the results from the previous model but we note that both models present different features; one slightly underestimates the cell volume and gives a too stiff elastic behaviour while the other does the opposite. To sum up, the model developed here cannot be considered as fully transferable to the ringwoodite's polymorphs since it generates an unstable structure for forsterite; however, it represents an alternative to the model of Price et al. (1987) for the simulation of wadsleyite when a softer description of the elastic behaviour is required.

Pressure effect

So far, the calculations reported were carried out at 0 K and 0 GPa but obviously it would be more appropriate to study ringwoodite within its stability field. In mantle minerals, pressure has a greater effect than temperature on many physical properties. Therefore, it is important to investigate the ability of the new model to reproduce the effect of pressure. The calculations were performed up to an isotropic external pressure of 30 GPa, which encompasses the stability field of ringwoodite (about 20 - 25 GPa at mantle temperatures). From the data of volume compression (Fig. 2), the pressure-dependence of the bulk-modulus was determined using two different equations of state (EOS). The EOS of Vinet et al. (1987), which has already been used by Matsui (1999) for ringwoodite, gives $(\partial \underline{K}/\partial \underline{P}) = 2.77$ for both spinels: γ-Mg_2SiO_4 and γ-Mg_2GeO_4. If we use the third-order Birch-Murnaghan EOS, then we find $(\partial \underline{K}/\partial \underline{P}) = 2.87$ and 2.86 for ringwoodite and magnesium germanate, respectively. For the pressure-dependence of the shear modulus, a second-order polynomial fitting is used. $(\partial \underline{\mu}/\partial \underline{P})$ is found to be equal to 0.37 and 0.27 for ringwoodite and magnesium germanate, respectively. First, the comparison of the predicted effect of pressure for both spinels shows that it is nearly the same for the pressure range investigated, even if the pressure derivative of the shear modulus is slightly lower for the germanate spinel. This supports the use of γ-Mg_2GeO_4 as an elastic analogue for the mantle ringwoodite. These results must also be compared to laboratory measurements. Several experimental studies have aimed to determine the elasticity of ringwoodite at highpressure and are reported in the literature. Among them, three studies display a large pressure range, from room pressure to 12, 16 or 30 GPa: Meng et al. (1994) obtained $(\partial \underline{K}/\partial \underline{P}) = 4.2(3)$ by measuring the static compression with X-ray diffraction (Fig. 2), Li (2003) found $(\partial \underline{K}/\partial \underline{P}) = 4.5(2)$ and $(\partial \underline{\mu}/\partial \underline{P}) = 1.5(1)$ by ultrasonic interferometry and Sinogeikin et al. (2003) measured $(\partial \underline{K}/\partial \underline{P}) = 4.1(3)$ and $(\partial \underline{\mu}/\partial \underline{P}) = 1.3(2)$ by Brillouin scattering. Within the experimental uncertainties, the different methods used are in good agreement. Figure 2 shows that up to 15 GPa the predicted

data of the compression volume are in relatively good agreement with the measurements. However, the calculated pressure derivatives of the elastic moduli on the whole pressure range investigated are too low compared to the observed data. Across the ringwoodite stability field, the model underestimates the effect of pressure, which is not totally surprising, as the potentials were fitted to room pressure data.

In the model described here, we took a potential with a harmonic form for the breathing shell (Eq. 4) although two other forms exist; the exponential and the single exponential forms which can respectively be written as follows:

$$U_i = K_i \left[\exp\left(\rho\left(R_i - R_0\right)\right) + \exp\left(-\rho\left(R_i - R_0\right)\right)\right]$$

$$U_i = K_i \exp\left(\rho\left(R_i - R_0\right)\right)$$

We have tested these two potential forms in order to see if they give a better description of ringwoodite's behaviour under highpressure. The parameters were fitted each time to the 0 GPa experimental data as with the harmonic potential. The accuracy of the description of data at zero pressure and the discrepancy as a function of pressure is strictly identical. Thus, changing the form of the breathing shell potential can bring no improvement to this model.

Intrinsic defects

The potential model derived here provides a good description of the spinel structure of ringwoodite and its germanium analogue and has been used to investigate the atomic defects within these minerals, which are of considerable interest because of their essential role in many geological processes. For instance, the viscosity and rheology of the Earth's mantle is likely to be controlled by diffusion, which in turn depends on the intrinsic disorder within the minerals. For this reason, calculations of formation and migration energies of these intrinsic defects are very important. Even if the description of the effect of pressure on the cell volume is correct up to 15

GPa, in a first step, we have chosen to limit our calculations to the zero pressure case, which is known to already give important information about the defect population.

For thermodynamic reasons, solids must always contain defects above absolute zero. We will focus here on intrinsic defects, i.e. vacancies and interstitials in thermodynamic equilibrium, which combine to form Schottky and Frenkel defects. A Schottky defect corresponds to charge-balanced vacancies in stoichiometric proportions (two Mg vacancies, one Si vacancy and four O vacancies in the case of ringwoodite), but partial Schottky defects can also be considered, like, for instance, one Mg vacancy associated with one O vacancy. The formation energy of these Schottky defects is equal to the sum of the energies of the vacancies involved plus the lattice energy of the phase removed to the crystal surface. In the case of Frenkel defects, vacancies are charge balanced by the formation of interstitials of the same species. The formation energy of Frenkel defects is then the sum of the individual vacancy and interstitial energies. The point defect energies are calculated using the Mott-Littleton method (Mott and Littleton 1938) implemented in GULP. It is an embedded regions technique with the point defect (vacancy or interstitial) at the centre. In the first spherical region around the defect, an explicit atomistic simulation is carried out to relax the atom positions to zero force. The radius of this region is chosen so that the effects of the defect are relatively weak at its boundary. The second region extends to infinity. Its inner part deals with short-range interactions, while in the outer part, only the polarisation is calculated. For further details of this methodology, see Gale and Rohl (2003).

The formation energies of Schottky and Frenkel defects are given in Table 6 for ringwoodite and the germanate spinel. The energies obtained for both spinels are relatively close but the most important result is that the relative order of the defects is nearly the same for both minerals. The small discrepancy corresponds to the three defects presenting formation energies around 9 eV per point defect. Thus according to these results, the germanate spinel is a good analogue for ringwoodite, from a defect population point of view. Furthermore, the MgO partial Schottky

defect displays the lowest energy per point defect, 7.06 and 7.09 eV for ringwoodite and the germanate spinel respectively. This suggests that, in the ideal case modelled here, the MgO Schottky defects where a Mg vacancy is charge balanced by an O vacancy will predominate. This result represents a first step for the understanding of the physical and chemical processes of the transition zone. It would be very interesting now to calculate the migration energies of these two defects in order to determine if diffusion occurs by a vacancy mechanism.

Conclusions

We have developed for ringwoodite and the germanate spinel, a new set of potentials which incorporate a breathing shell model. For both spinels, this allows the accurate description of the structural parameters as well as the elastic constants for 0 to about 15 GPa; however above these pressures, the compressibility is underestimated. This potential model is also transferable to wadsleyite, for which the accuracy of the description of the structural and elastic parameters is as good as that of the model of Price et al. (1987) but the structure calculated displays a softer elastic behaviour. The accuracy gained for the description of spinel-phases enables us to investigate the energetic of point defects and especially the incorporation of water (hydrogen associated to point defects). But beyond this application, the ability to model intrinsic defects is of considerable importance since they control most of the mineral properties (diffusion, electrical conduction, viscosity). In order to understand the mechanisms governing these properties, we must know the nature of the defects, their concentration and their mobility. A first step has been done, here, by determining, from the calculated formation energies, that the MgO Schottky defects are most favourable.

Acknowledgements This study was partially supported by the EU through the Human Potential Program HPRM-CT-2000-0056. We thank A. Walker,A. Gatzemeier and two anonymous reviewers for their helpful discussions and remarks. KW would like to thanks the Royal Society for funding and JDG gratefully acknowledges the support of the Government of Western Australia through a Premier's Research Fellowship. We also thank EPSRC for provision of computing resources under grant no. GR/SO6233/01.

References

Brodholt J (1997) Ab initio calculations on point defects in forsterite (Mg_2SiO_4) and implications for diffusion and creep. Am Mineral 82: 1049-1053

Catlow CRA, Kotomin E (2003) Computational Materials Sciences. NATO Science Series III: Computer and Systems Sciences. 187. IOS Press, Netherlands

Catlow CRA, Price GD (1990) Computer modelling of solid-state inorganic materials. Nature 347: 243-248

Catlow CRA, Faux ID, Norgett MJ (1976) Shell and breathing shell model calculations for defect formation energies and volumes in magnesium oxide. J Phys C: Solid State Physics 9: 419-429

Dachille F, Roy R (1960) Am J Sci 258: 225-246

Dick BG, Overhauser AW (1958) Theory of the dielectric constants of alkali halide crystals. Phys Rev 112: 90-103

Fujino K, Sasaki S, Takeuchi Y, Sadanaga R (1981) X-ray determination of electron distributions in forsterite, fayalite and tephroite. Acta Crystallogr Sect. B 37: 513-518

Gale JD (1997) GULP: A computer program for the symmetry-adapted simulation of solids. J Chem Soc Faraday Trans 93: 629-637

Gale JD, Rohl AL (2003) The General Utility Lattice Program (GULP). Mol Simula 29: 291-341

Haiber M, Ballone P, Parrinello M (1997) Structure and dynamics of protonated Mg_2SiO_4: An ab-initio molecular dynamics study. Am Mineral 82: 913-922

Horiuchi H, Sawamoto H (1981) β–Mg_2SiO_4: single-crystal X-ray diffraction study. Am Mineral 66: 568-575

Isaak DG, Anderson OL, Goto T, Suzuki I (1989) Elasticity of single-crystal forsterite measured to 1700 K. J Geophys Res 94: 5895-5906

Leslie M (1989) Calculation of the energies of point defects in quartz. J Chem Soc Faraday Trans 85: 404-413

Lewis GV, Catlow CRA, Cormack AN (1985) Defect structure and migration in Fe_3O_4. J Phys Chem Solids 46: 1227-1233

Li B (2003) Compressional and shear wave velocities of ringwoodite γ-Mg_2SiO_4 to 12 GPa. Am Mineral 88: 1312-1317

Madden PA and Wilson M (1996) Covalent effects in "ionic" systems. Chem. Soc.Review. 339-350.

Matsui M, Busing WR (1984) Computational modeling of the structure and elastic constants of the olivine and spinel forms of Mg_2SiO_4. Phys Chem Miner 11: 55-59

Matsui M (1999) Computer simulation of the Mg_2SiO_4 phases with application to the 410 km seismic discontinuity. Phys Earth Planet Int 116: 9-18

Meng Y, Fei Y, Weidner DJ, Gwanmesia GD, Hu J (1994) Hydrostatic compression of γ–Mg_2SiO_4 to mantle pressures and 700 K: thermal equation of state and related thermoelastic properties. Phys Chem Miner 21: 407-412

Mott NF, Littleton MJ (1938) Conduction in polar crystals. I. Electrolytic conduction in solid salts. Trans Faraday Soc 34: 485

Price GD, Parker SC (1984) Computer simulations of the structural and physical properties of the olivine and spinel polymorphs of Mg_2SiO_4. Phys Chem Miner 10: 209-216

Price GD, Parker SC, Leslie M (1987) The lattice dynamics and thermodynamics of the Mg_2SiO_4 polymorphs. Phys Chem Miner 15: 181-190

Purton J, Catlow CRA (1990) Computer simulation of feldspar structures. Am Mineral 75: 1268-1273

Ringwood AE (1975) Composition and petrology of the Earth's mantle. New York: Mc Graw-Hill

Sasaki S, Prewitt CT, Sato Y, Ito E (1982) Single-crystal X ray study of γ Mg_2SiO_4. J Geophys Res 87: 7829-7832

Sawamoto H, Weidner DJ, Sasaki S, Kumazawa M (1984) Single-crystal elastic properties of the modified spinel (Beta) phase of magnesium orthosilicate. Science 224: 749-751

Schroeder U (1966) A new model for lattice dynamics (breathing shell model). Solid State Com 4: 347-349

Sinogeikin SV, Bass JD, Katsura T (2003) Single-crystal elasticity of ringwoodite to high pressures and high temperatures: implications for 520 km seismic discontinuity. Phys Earth Planet Int 136; 41-66

Stillinger F, Weber TA (1985) Computer simulation of local order in condensed phases of silicon. Phys Rev B 31: 5262-5271

Vinet P, Ferrante J, Rose JH, Smith JR (1987) Compressibility of solids. J Geophys Res 92: 9319-9325

Von Dreele RB, Navrotsky A, Bowman AL (1977) Refinement of the crystal structure of Mg_2GeO_4 spinel. Acta Crystallogr B33: 2287-2288

Walker AM, Wright K, Slater B (2003) A computational study of oxygen diffusion in olivine. Phys Chem Miner 30: 536-545

Weidner DJ, Hamaya N (1983) Elastic properties of the olivine and spinel polymorphs of Mg2GeO4 and evaluation of elastic analogues. Phys Earth Planet Int 33: 275-283

Weidner DJ, Sawamoto H, Sasaki S (1984) Single-crystal elastic properties of the spinel phase of Mg_2SiO_4. J Geophys Res 89: 7852-7860

Wright K, Catlow CRA (1994) A computer simulation study of (OH) defects in olivine. Phys Chem Miner 20: 515-518

Wright K, Catlow CRA (1996) Calculations on the energetics of water dissolution in wadsleyite. Phys Chem Miner 23: 38-41

Wright K, Freer R, Catlow CRA (1995) Oxygen diffusion in grossular and some geological implications. Am Mineral 80: 1020-1025

Yoneda A (1990) Pressure derivatives of elastic constants of single crystal MgO and $MgAl_2O_4$. J Phys Earth 38: 19-55

Figure captions

Fig. 1 Description of the breathing shell model. q_c, q_s, K_{BSM} and $k_{C\text{-}S}$ represent the charges of the core and shell, and the spring constants of the breathing shell and the core-shell interaction, respectively

Fig. 2 Volume compression: the symbols are the observed hydrostatic compression data at 300 K from Meng et al. (1994), the solid line is our calculated curve for ringwoodite and the dashed line for germanate spinel

Table 1 Calculated and observed properties of γ–Mg_2SiO_4. A is the cell parameter (Å), $\underline{V}$, the cell volume (Å^3), $\underline{C}_{ij}$, the elastic constants and $\underline{K}$, $\underline{\mu}$, the bulk and shear moduli respectively (GPa). Numbers in parenthesis are the differences between calculations and experiment (%). Observed data from Sasaki et al. (1982) and Weidner et al. (1984)

	Obs.	Price et al. (1987)	This study
a	8.065	8.016 (-0.60)	8.066 (0.01)
V	524.6	515.1 (-1.81)	524.8 (0.04)
C_{11}	327.0	412.9 (26.27)	327.1 (0.03)
C_{44}	126.0	136.7 (8.49)	126.3 (0.24)
C_{12}	112.0	169.5 (51.34)	111.1 (-0.80)
K	184.0	250.6 (36.20)	183.1 (-0.49)
μ	119.0	130.3 (9.50)	118.3 (-0.59)

Table 2 Parameters of the potential model used in this study. Equations are given in the text

Charges				
Ions	Core	Shell		
Mg	2.000			
Si	4.000			
Ge	4.000			
O	0.800	-2.800		
Buckingham potential	A (eV)	ρ (Å)	C (eVÅ^6)	Cutoffs (Å)
Mg-O	31.326316	0.30599	0.00000	10.0
Si-O	173.76200	0.14949	0.00000	12.0
Ge-O	327.41125	0.14045	0.00000	12.0
O-O	0.431x10^{-7}	0.30000	48.28154	16.0
Breathing shell model: (harmonic form)	K_i (eV)		R_0 (Å)	
O-O	342.7170		1.20000	0.1
Core-shell spring constant	k_i (eVÅ^{-2})			
O-O	49.214316			

Three-body potential: Stillinger-Weber	k_{ijk} (eV)	θ_0 (°)	ρ_{ij}	ρ_{ik} (Å)	ij	ik	jk
Si-O-O	69.2069	109.470	2.0	2.0	3.0	3.0	6.0
Ge-O-O	83.0034	109.470	2.0	2.0	3.0	3.0	6.0

Table 3 Calculated and observed properties of γ–Mg_2GeO_4. Same legend as Table 1. Observed data from Von Dreele et al. (1977), and Weidner and Hamaya (1983)

	Obs.	This study
a	8.249	8.250 (0.01)
V	561.3	561.5 (0.04)
C_{11}	300.2	300.0 (-0.07)
C_{44}	125.7	126.0 (0.23)
C_{12}	118.4	118.0 (-0.34)
K	179.0	179.0 (0.00)
μ	109.0	110.0 (+0.92)

Table 4 Calculated and observed properties of periclase (MgO). Same legend as Table 1. Observed data from Yoneda A (1990)

	Obs.	This study
a	4.217	4.277 (1.42)
V	74.99	78.24 (4.33)
C_{11}	297.8	298.4 (0.20)
C_{44}	155.8	148.1 (-4.94)
C_{12}	95.1	90.5 (-4.84)
K	162.7	159.8 (-1.76)
μ	131.1	126.6 (-3.42)

Table 5 Calculated and observed properties of forsterite and wadsleyite. Same legend as Table 1. Observed data from Fujino et al. (1981), Issak et al. (1989) for forsterite and Horiuchi and Sawamoto (1981), Sawamoto et al. (1984) for wadsleyite

	Forsterite			Wadsleyite		
	Obs.	Price et al. (1987)	This study	Obs.	Price et al. (1987)	This study
a	4.753	4.782 (0.61)	4.846 (1.94)	5.698	5.651 (-0.82)	5.712 (0.35)
b	10.19	10.25 (0.59)	10.26 (0.66)	11.44	11.39 (-0.44)	11.40 (-0.51)
c	5.978	5.986 (0.13)	5.964 (-0.24)	8.257	8.275 (0.22)	8.359 (1.29)
V	289.5	293.3 (1.31)	296.4 (2.40)	538.1	532.6 (-1.02)	544.4 (1.16)
C_{11}	330.0	358.6 (9.53)	282.0 (-14.54)	360.0	434.6 (20.72)	353.2 (-1.89)
C_{22}	200.0	206.6 (3.33)	159.5 (-20.25)	383.0	425.6 (11.12)	382.8 (-0.05)
C_{33}	236.0	281.1 (19.11)	231.0 (-2.12)	273.0	331.7 (21.50)	218.5 (-19.96)
C_{44}	67.0	44.2 (-34.03)	289.9 (332.69)	112.0	101.6 (-9.29)	100.8 (-10.00)
C_{55}	82.0	74.5 (-9.15)	80.4 (-1.95)	118.0	113.5 (-3.81)	97.9 (-17.03)
C_{66}	81.0	84.3 (4.07)	75.4 (-6.91)	98.0	100.6 (2.65)	96.1 (-1.94)
C_{12}	66.0	93.8 (42.12)	54.7 (-17.12)	75.0	118.6 (58.13)	66.9 (-10.80)
C_{13}	68.0	96.2 (41.47)	46.0 (-32.35)	110.0	136.2 (23.82)	82.2 (-25.27)
C_{23}	72.0	87.7 (21.81)	51.7 (-28.19)	105.0	144.1 (37.24)	91.7 (-12.67)
K	129.5	147.9 (14.2)	103.7 (-19.92)	174.0	219.1 (25.92)	152.2 (-12.53)
μ	81.1	70.9 (-12.58)	92.4 (13.93)	114.0	112.8 (-1.05)	101.7 (-10.79)

Table 6 Formation energies of the intrinsic defects in ringwoodite and the germanate spinel. In order to allow the direct comparison, energies are expressed per point defect (eV)

	γ-Mg_2SiO_4	γ-Mg_2GeO_4
Mg_2SiO_4 Schottky	9.26	9.04
MgO Schottky	7.06	7.09
SiO_2 Schottky	12.15	11.80
O Frenkel	9.35	9.41
Mg Frenkel	9.46	8.94
Si Frenkel	22.63	21.30

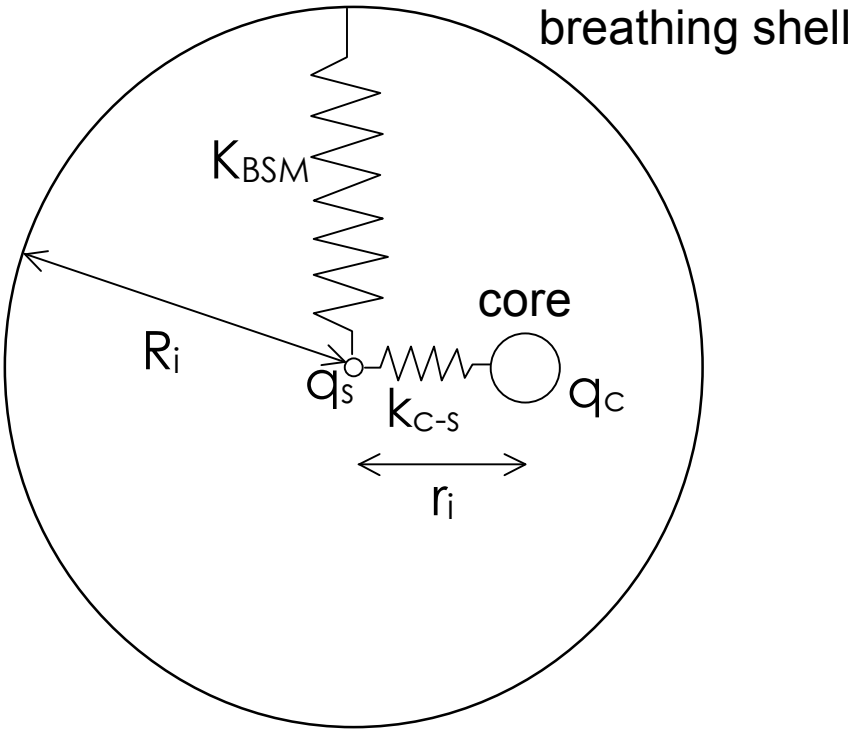

Fig. 1

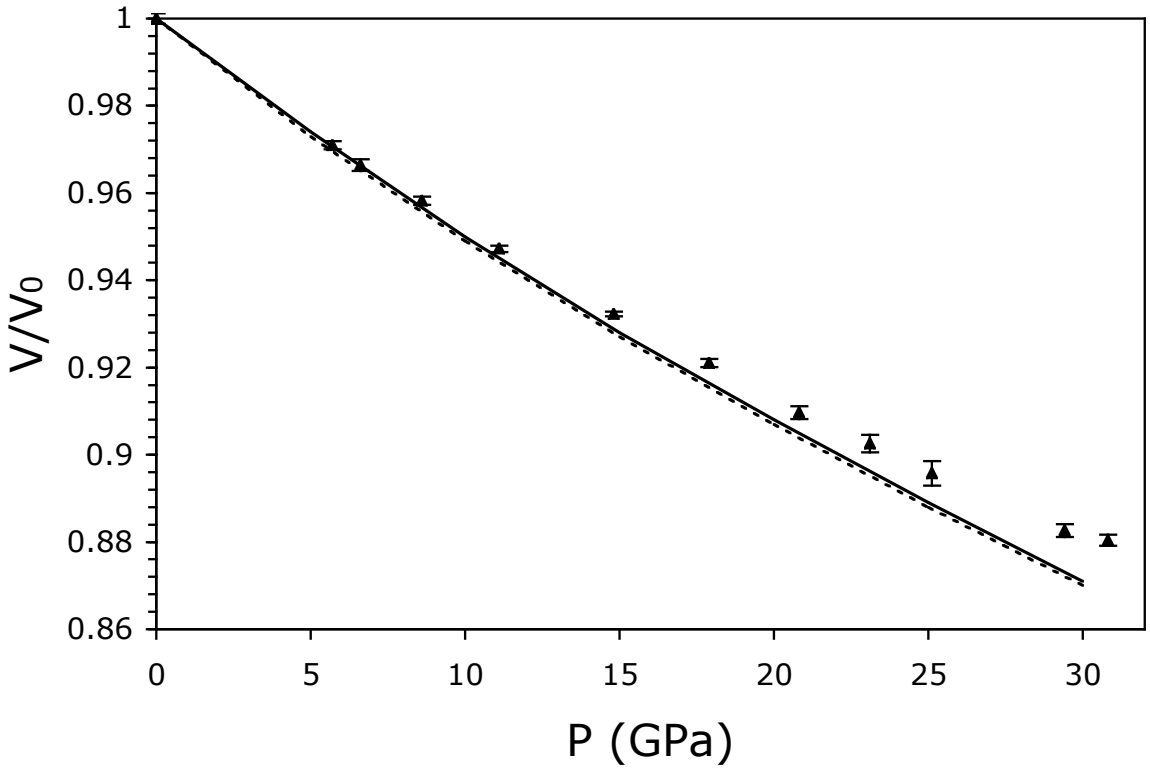

Fig. 2